

Electrochemical Behavior of API X80 Steel in Acidic Soils from Southeast China

Maocheng Yan^{1,*}, Cheng Sun¹, Jin Xu¹, Wei Ke¹

¹ Environmental Corrosion Center, Institute of Metal Research, Chinese Academy of Sciences, 62 Wencui Rd, Shenyang 110016, China

*E-mail: Yanmc@imr.ac.cn, Yanmc@gmail.com

Received: 15 August 2014 / Accepted: 17 November 2014 / Published: 30 December 2014

Acid soils in Southeast China are known as one kind of the most corrosion aggressive soils toward pipeline steels. Acid soils have high contents of Fe oxides, especially their electrochemically active phase, like ferrihydrite and lepidocrocite, which will influence corrosion process and induce some new phenomena in the soil corrosion. In this work, Fe oxides residing in the clay minerals of an acidic soil were characterized by XRD and cyclic voltammetry. The electrochemical behavior of API X80 pipeline steel in the soil was evaluated by EIS and Tafel polarization. Cyclic voltammetry shows that Fe oxides were electrochemically active. Redox active nature Fe oxides and their phase transformation occurring in the soil are suggested to simulate the steel corrosion, and a possible electrode reaction series involved in the corrosion process is proposed.

Keywords: API X80 Steel; Acidic soil; Corrosion; Fe oxide; EIS

1. INTRODUCTION

Although coatings and cathodic protection (CP) are generally combined for external protection of buried pipelines, external corrosion by soil is still one of leading causes of leaks and ruptures of pipelines [1-5]. Corrosion of pipeline steel has been widely studied in various media, such as soil leaching solutions, $\text{CO}_3^{2-}/\text{HCO}_3^-$ solutions or dilute bicarbonate solutions simulating electrolytes trapped under disbonded coating [6]. The methodology only focuses on dissolved ions and takes the soil as inert particles. They cannot explain variations in soil corrosion due to neglecting the multiphase nature of the soil and interplays between the colloidal soil particle and the charged metal.

Generally, corrosion of pipeline steel is moderate in well-drained soil with a high resistivity [7]. Acidic soils in Southeast China, as well as saline soils in Western China, are listed as the typical highly corrosive soils for pipeline steels in China, evidenced by a series of long-term field exposure

test in Southeast China [8-10]. Several important nature-gas pipelines, e.g. the west-east pipeline II and the China-Burma pipeline, pass through the acidic soil region in Southeast China. Severe corrosion attack has been observed under coating defects where CP fails in field inspection in the acidic soil region in Southeast China. Now, there is growing safety and economic concern about the corrosion risk of pipeline in the acidic soil region.

It has been recognized that steel corrosion in acidic soil exhibits specific properties and the mechanism involved is different from that in the common soils [9]. But so far, satisfactory interpretation for the phenomenon has not yet been proposed due to complexity of the soil corrosion system. Recent work in our laboratory indicates that Fe oxide, as the most electrochemically reactive component of the soil, is crucial for the corrosion process in acidic soils [6]. However, a process-based understanding of the corrosion process under the influence of Fe oxides is still lacking because much detailed information about the principal reactions involved is still not available.

The present study involves identification of the phase composition of Fe oxides in a typical acidic soil collected from Southeast China and electrochemical measurements for API X80 pipeline steel in the acidic soil. The aim of this work is to provide a better understanding of the property and nature of steel corrosion in the presence of the soil Fe oxides. A particular attention was paid to the influence of the redox active Fe oxide and kinetics and mechanism involved in the corrosion process are proposed.

2. EXPERIMENTAL

2.1 Materials and electrode preparation

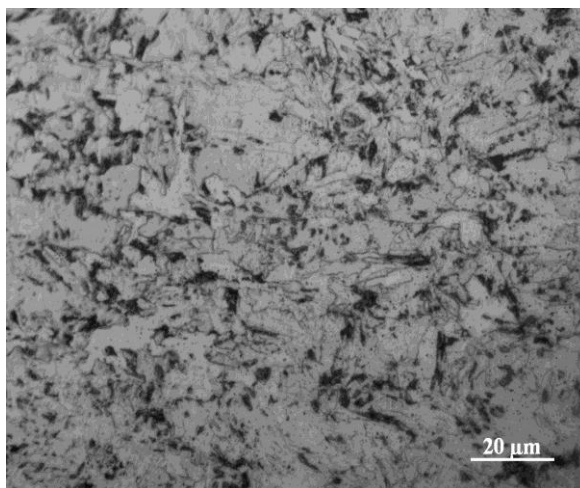


Figure 1. Optical metallurgical structure of the X80 pipeline steel, displaying an acicular ferrite dominated matrix microstructure

The test material was API X80 pipeline steel with the composition as follows (wt%): C 0.07, Mn 1.82, Si 0.19, P 0.007, S 0.023, Cr 0.026, Ni 0.17, Cu 0.020, Al 0.028, Mo 0.23, Ti 0.012, Nb

0.056, V 0.002, N 0.004, B 0.0001. The optical metallurgical structure of the X80 pipeline steel is shown Fig. 1, which displays an acicular ferrite dominated matrix microstructure characterized by the fine non-equiaxed ferrite. A remarkable characteristic of this type of microstructure possesses a unique and irregular configuration, which has various size grains distributed in a chaotic manner with random orientations [11].

The rectangular coupon is the size of $10 \times 10 \times 3$ mm was cut from steel plates and soldered to a Cu wire for electrical connection. The sample acting as a working electrode was embedded in epoxy resin to give a working area of 1 cm^2 for electrochemical measurement. The working surface was abraded to 1000 grit silicon carbide (SiC) paper followed by cleaning in deionized water and alcohol and then air dried.

2.2 Acidic soil and characterization

The acidic soil was collected at the Red Soil Ecological Experiment Station ($28^{\circ}15' \text{ N}$, $116^{\circ}55' \text{ E}$) in Yingtan, Southeast China. The typical subtropical humid monsoon climate prevails this area, with an annual mean temperature of $18 \text{ }^{\circ}\text{C}$, abundant annual rainfall (1750 mm) [12]. Yingtan is a typically hilly region of acidic soil in subtropical China. The acidic red soil is Ultisol according to the USDA soil taxonomy [13]. The soil sample was air-dried, ground and passed through a 2 mm sieve. Some chemical and physical properties of the soil are given in Table 1.

Table 1. Physicochemical properties of the acidic soil used in this study

Soil type	Ultisol
Organic matter ^a (wt %)	0.37
Total nitrogen (wt %)	0.025
pH (soil water ratio 1:2.5)	3.95
Total salt (wt %)	0.0042
Free Fe ₂ O ₃ ^b g/kg	49
Exchangeable acid (cmol/kg)	3.93
Conductivity (mS/cm)	
Slurry (soil water ratio 1:0.5)	0.018
Leaching solution (soil water ratio 1:5)	0.011
Ionic composition (wt %)	
NO ₃ ⁻	0.0006
Cl ⁻	0.0007
SO ₄ ²⁻	0.001
HCO ₃ ⁻	0.0011
Ca ²⁺	0.0004
Mg ²⁺	0.0002
K ⁺	0.0001
Na ⁺	0.0001

^a Organic matter, determined by dichromate method.

^b Determined by the dithionite-citrate-bicarbonate (DCB) method.

To characterize the influence of Fe oxides, a part sample of the red soil was treated by a dithionite-citrate buffer solution (0.3 M sodium citrate + 0.05 M citric acid + 0.14 M sodium dithionite) to remove Fe oxides in the soil [14, 15]. The detailed procedure of the Fe oxide removal treatment can be found in Ref. [10].

The <2 μm clay fraction were separated from the bulk soil by gravity settling in water under slightly alkaline conditions. The mineralogical composition (as opposed to elemental composition) of the clay fraction powder was analyzed by X-ray diffraction (XRD). The electrochemical activity of the soil iron oxides was characterized by cyclic voltammetry measured on a Pt foil electrode (area 0.16 cm^2) at the scan rate 1mV s^{-1} . The cyclic voltammetry was conducted by an EG&G Parstat 2273 potentiostat using a traditional three-electrode electrochemical cell system.

2.3 Exposure tests and electrochemical corrosion measurements

The soil exposure test and electrochemical measurement was performed in a cylindrical plastic cell at a water content of 25 wt % (dry weight basis). The water holding capacity (the saturated water content) of the acidic soil is *ca* 30.1 %. All the coupons were buried *ca*. 25 cm beneath the surface of soils. The soil cells were placed in humidity chambers throughout the test to keep the water content level of the soils. The experiments were performed for 45 days at the room temperature.

The electrochemical measurements were carried out periodically by an EG&G Parstat 2273 potentiostat using a traditional three-electrode electrochemical cell system. The cell consisted of steel sample with an exposure area of 1.0 cm^2 as working electrode and a saturated calomel electrode (SCE, 0.241 V vs standard hydrogen electrode [SHE]) was used as reference electrode (RE). A graphite plate (50 cm^2) worked as a counter electrode. The RE was placed *ca* 5 cm from the surface of the working electrode through a Luggin probe. It was not placed any nearer from the working electrode to avoid any contamination from chlorides. EIS spectra were acquired at open circuit potential (OCP) over the frequency range of 10^5 – 10^{-2} Hz under excitation of a sinusoidal perturbation signal of 5 mV amplitude. Tafel plots were measured on separate electrodes after 1-day and 45-day exposure. The Tafel plots were recorded potentiodynamically from -0.25 V to $+0.25\text{ V}$ vs OCP at the scan rate of 0.166 mV s^{-1} .

All the electrochemical experiments were repeated three times and the typical results were reported in this paper.

Due to specificity of the soil media, validation of the EIS spectra was performed by several means including checking the stability of the system, i.e., hysteresis between the spectra acquired by high-to-low and low-to-high frequency sweeps, the linearity of the system, i.e., measuring the spectra at AC signal amplitudes between 2 and 10 mV (rms), as well as a Kramers–Kronig (K-K) transform test. K-K transform was performed by an Echem Analyst software (V 5.5) based on the procedure of Boukamp [14].

2.5 Characterization of corrosion surface

The surface morphologies of steel samples retrieved after 45 day exposure in the soil were analyzed by an optical microscope and by a scanning electron microscope (SEM, Philips FEG XL30).

3. RESULTS

3.1 Properties of the clay fraction in the acidic soil

Figure 2 presents the XRD pattern of the $< 2 \mu\text{m}$ clay fraction of the acidic soil. The dominant clay minerals are kaolinite. Diffraction peaks associated to goethite ($\alpha\text{-FeOOH}$) and hematite ($\alpha\text{-Fe}_2\text{O}_3$) are observed in the XRD pattern. The characteristic diffraction pattern of ferrihydrite can also be distinguished in the diffractogram. Ferrihydrite is usually designated in the XRD by the number of peaks corresponding to d-values varying between 0.15–0.25 nm, for example, the so called 2-line ferrihydrite (2LFh) and 6-line ferrihydrite (6LFh) are known as its most occurring forms [15].

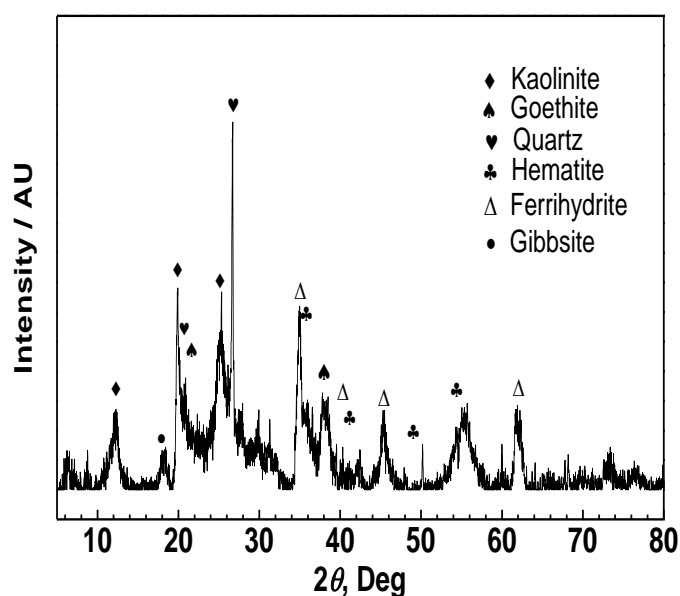


Figure 2. X-ray diffraction pattern of the $< 2 \mu\text{m}$ clay fraction of the acidic soil from Yingtan, Southern China

The cyclic voltammetry of the clay fraction of the acidic soil measured on an inertia Pt foil is shown in Fig. 3. The cyclic voltammetry shows that the Fe oxides are electrochemically active. The reduction peak in the vicinity of -0.75 V vs SCE and oxidation peak near -0.64 V vs SCE associated to the Fe oxide residing in the soil can be clearly identified in the cyclic voltammetry plot. After Fe oxide was removed from the soil, the reduction-oxidation is absent.

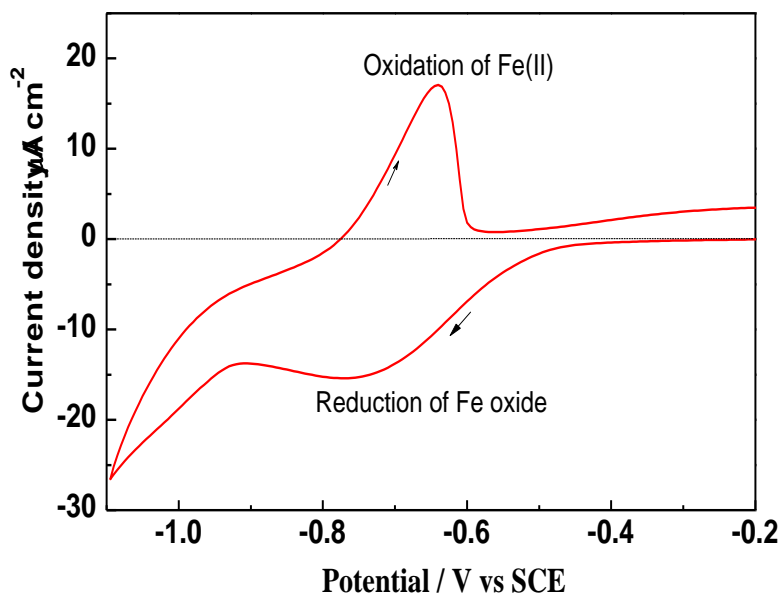


Figure 3. Cyclic voltammety (scan rate 1 mV s^{-1}) of the clay fraction in the acidic soil measured on a Pt foil (area 0.16 cm^2)

3.2 Tafel plots

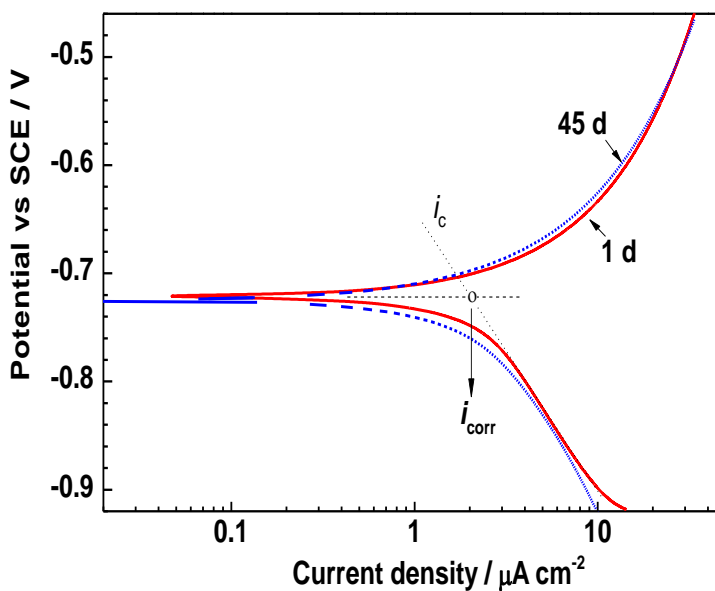


Figure 4. Tafel polarization plot for X80 pipeline steel in acidic soil after 1 day and 45 day exposure in the acidic soil (Potential scan rate 0.166 mV s^{-1})

Tafel plots for the X80 steel after 1 and 45 day exposure in the acidic soil are presented in Fig. 4. Table 2 gives average values of the corrosion current and corrosion potential for the X80 steel after 1 and 45 day exposure. The OCP of the steel is -720 mV, and it keeps relatively stable during the test. The corrosion process of the steel is under activation control, and the Tafel equation can be applied for this system,

$$\eta_c = E - E_{\text{corr}} = \beta_c \ln \frac{i_c}{i_{\text{corr}}} \quad (1)$$

where η_c is the activation overpotential, β_c is the cathodic Tafel slope.

The corrosion current density i_{corr} can be determined by Tafel extrapolation cathodic [16]. Cathodic branch of Tafel plots were extrapolated to get a fitting line of cathode current i_c and the i_c value at the OCP is i_{corr} , as schematically shown in Fig. 4. The i_{corr} values for the X80 steel in the acidic soil are $2.02 \mu\text{A}/\text{cm}^2$ (0.024 mm/a) at the initial and $1.83 \mu\text{A}/\text{cm}^2$ (0.021 mm/a) after 45 day exposure.

Table 2. Corrosion parameters from analysis of Tafel plots for X80 steel in acidic soil

Time (day)	E_{corr} (mV)	I_{corr} ($\mu\text{A cm}^{-2}$)	β_a (mV dec ⁻¹)	β_c (mV dec ⁻¹)
1	-0.721	2.02	130	277
45	-0.726	1.83	177	309

3.3 Validity of EIS measurements

EIS has been shown to be a useful tool to obtain corrosion process related electrochemical parameters for studying soil corrosion mechanism. Characteristics of both electrochemical process and physical processes of the corrosion system in soils can be reflected by EIS [17]. Electrochemical measurements in soils have been challenging due to the inherent characteristics of soils, like the high resistivity and the instinctive capacitance of soil media. For EIS measurement in the highly resistive soil, stability of the measured system is crucial to obtain reliable EIS data [18]. In this work, the stability of the test system and validity of the EIS measurement were checked by several methods including the hysteresis between the spectra acquired by high-to-low and low-to-high frequency sweeps, the spectra acquired at different amplitudes of the AC signal between 2 and 20 mV (rms) and the K–K transform.

EIS plots acquired by high-to-low and low-to-high frequency sweeps almost exactly coincide. Good agreement is also observed between the spectra acquired by at different amplitudes of the AC signal between 5 and 20 mV (rms). These EIS plots are not shown in this paper. The impedance is defined within Linear System Theory (LST). According to constraints of LST, linearity, causality and stability constraints must be satisfied for a system for validity of EIS measurements [18]. The K–K transform is a convenient method to validate the measured EIS and examine the system with respect to causality, linearity, and stability constraints [19-21].

A set of data from K–K transform for EIS measured at both the beginning and the end of the exposure in the soil are shown in Fig. 5 as fitting lines on the measured EIS data. The experimental and the transformed impedance data for both the real and the imaginary components coincide remarkably, except for some disorder data points of measured EIS data. The similar agreement level is found for all EIS data in this work, which shows that the system under investigation satisfies constraints of LST and thereby validates the measured EIS data.

3.4 Electrochemical Impedance Spectroscopy Analysis

Evolution of EIS plots for the X80 steel in the acidic soil is shown in Fig. 6. *Two stages are clearly* seen from the evolution of EIS plots. In the first 10 days, Nyquist plots for the steel in the acidic soil are featured by an intact flattened semicircle at the low frequency region and a capacitive “tail” at the high frequencies ($f > 10^4$ Hz). The depressed semicircle at the low frequencies is also revealed by the existence of the maxima in the phase angle plot and the slope in the modulus plot in the vicinity of 0.2 Hz. The low frequency semicircle has the center under the real axis, displaying a frequency dispersion effect that is typical in EIS of solid metal electrodes. The low frequency semicircle keeps intact and its size maintains constant during the first 10 days exposure. The diameter of the low frequency semicircle increases on the 15 day and the low frequency semicircle gradually evolves to a straight line on the 30 day, whereas, the high frequency capacitive “tail” keeps constant and its overall profile does not change evidently throughout the exposure.

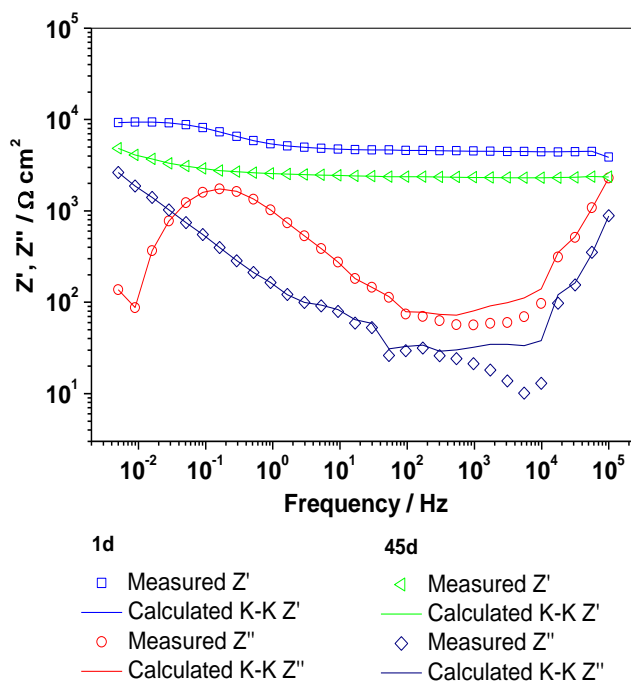


Figure 5. Kramers–Kronig transforms (the lines) of measured EIS data (the scatters) for X80 steel after 1 day and 45 day exposure in the acidic soil. The remarkable coincidence of the measured data and the transformed data exhibits that the system obeys the LST rule

The evolution of EIS plots indicates that the control process of the X80 steel corrosion in the acidic soil is changing from the activation control during the initial 10 days to a combination of the activation and the diffusion control. The 45° line in the low-frequency region shows the typical characteristics of the Warburg impedance, which generally reflects the diffusion process within the bulk soil. This can be attributed to the depletion of oxidizing agents surrounding the steel electrode and to the accumulation of corrosion product on the surface of the steel electrode.

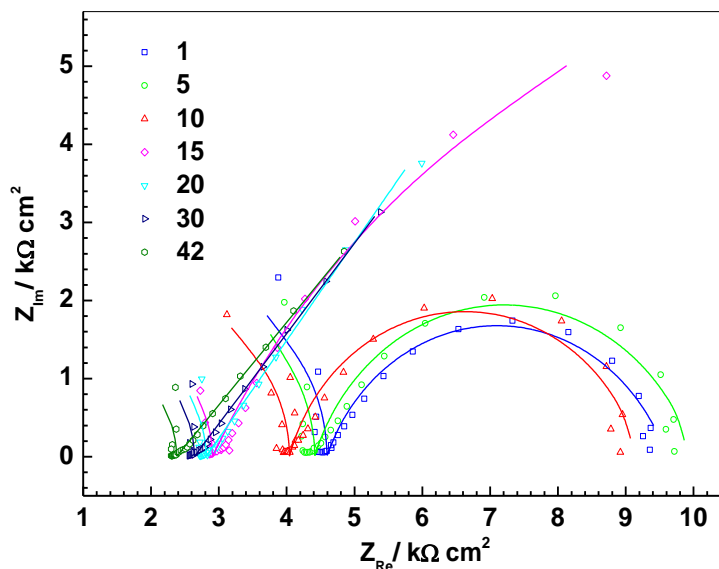


Figure 6. Evolution of Nyquist plot for X80 pipeline steel in the acidic soil

It should be specified that the appearance of the high frequency capacitive “tail” are commonly observed at the high–frequencies in EIS spectra measured in soil media. However, the observed capacitive “tail” in EIS in soil is rarely discussed in the lecture. The capacitive “tail” appears just from the beginning of the test and its overall profile does not vary obviously with the exposure period. Based on these features, in this work, the high frequency capacitive “tail” is associated with the response of the bulk soil which has its own dielectric property (capacitive behavior) and the capacitance is a function of the moisture content and clay content [22, 23].

The Nyquist plots present a distinct tendency to shift to left side in the complex plane during the exposure. In general, the low frequency impedance is dominated by the electrode control process, e.g. the charge transfer resistance (characterizing the corrosion process) or the diffusion impedance. Meanwhile, the soil resistance R_s corresponds to the real part of the impedance as the frequency tends to infinite. The low frequency semicircle is associated with the corrosion processes in the soil/steel interface and has been represented by a pair $Q_{dl}R_{ct}$ in parallel (Fig. 7), from which many kinetic parameters of the electrochemical process can be identified and quantified [24, 25]. During the exposure, both the modulus and phase angle peak at low-frequency vary upon the exposure time, indicating variation of corrosion processes and electrochemical kinetics. The evolution of R_{ct} and Q_{dl}

can be used to describe the corrosion process the steel, for instance, for the sake of convenience, the reciprocal of polarization resistance R_{ct}^{-1} can be generally used as an index of the corrosion rate. The characteristic frequency f_{max} regularly shifts to the low frequency, with the magnitude increasing.

The equivalent electrical circuit (ECC) shown in Fig. 7 was used to characterize the corrosion system, fit the EIS diagrams and extract some corrosion kinetic parameters. The circuit consists of soil resistance R_s , soil capacitance C_s , charge transfer resistance R_{ct} , and a constant phase element (CPE) Q_{dl} is used as a substitute of the ideal double layer capacitance C_{dl} at the metal/soil interface due to the non-ideal capacitive response of the interface. The impedance of Q is defined as [23, 26]:

$$Z_Q = [Y_0 (j\omega)^n]^{-1} \tag{2}$$

where ω is the angular frequency (s^{-1}), Y_0 the CPE constant (the admittance magnitude of the CPE) which can be converted into a capacitance, n the Q -power ($0 < n \leq 1$), and j the imaginary unit ($j^2 = -1$). Depending on the n value, Q reduces to a resistance ($Z_Q = R, n = 0$), a capacitor ($Z_Q = C, n = 1$), or a Warburg element ($Z_Q = W, n = 0.5$).

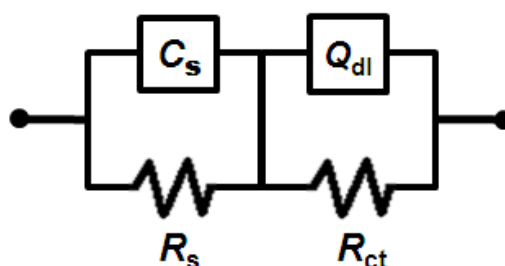


Figure 7. The equivalent circuit (CR)(QR) used to fit EIS data for X80 pipeline steel, where R_s represents the soil resistance, R_{ct} is the charge transfer resistance, and CPE Q_{dl} is used as a substitute of the double layer capacitance at the metal/soil interface due to the non-ideal capacitive response of the soil/steel interface

Corrosion kinetic parameters derived from EIS fitting by the equivalent circuit model (CR)(QR) are given in Table 3. The evolutions R_s and R_{ct} obtained by EIS fitting are plotted against time and given in Fig. 8. As can be seen, the value of R_{ct} of the steel increases from 4.4 $k\Omega\ cm^2$ at the initial of the test to 7.5 $k\Omega\ cm^2$ at the 45 day. Correspondingly, the corrosion rate R_{ct}^{-1} displays a clear decrease pattern with the duration of the exposure, as shown in Fig. 9, which indicates that cathodic depolarizers surrounding the electrode is depleted and corrosion product on the electrode surface is formed with extension of the exposure.

Table 3. Fitted EIS parameters of X80 pipeline steel during exposure in the acidic soil

Time (day)	R_s ($k\Omega\ cm^2$)	C_s ($\mu F\ cm^{-2}$)	R_{ct} ($k\Omega\ cm^2$)	Q_{dl}	
				Y_0 ($S\ s^n\ cm^{-2}$)	n
1	4.592	1.690×10^{-4}	4.592	1.66×10^{-4}	0.765
5	4.412	1.501×10^{-4}	5.597	1.905×10^{-4}	0.7878

10	4.039	2.041×10^{-4}	5.166	2.391×10^{-4}	0.8106
15	2.904	1.579×10^{-4}	6.727	1.150×10^{-3}	0.6806
20	2.811	1.725×10^{-4}	6.873	1.535×10^{-3}	0.5712
30	2.636	1.797×10^{-4}	7.128	1.627×10^{-3}	0.5462
45	2.375	2.061×10^{-4}	7.518	1.712×10^{-3}	0.5186

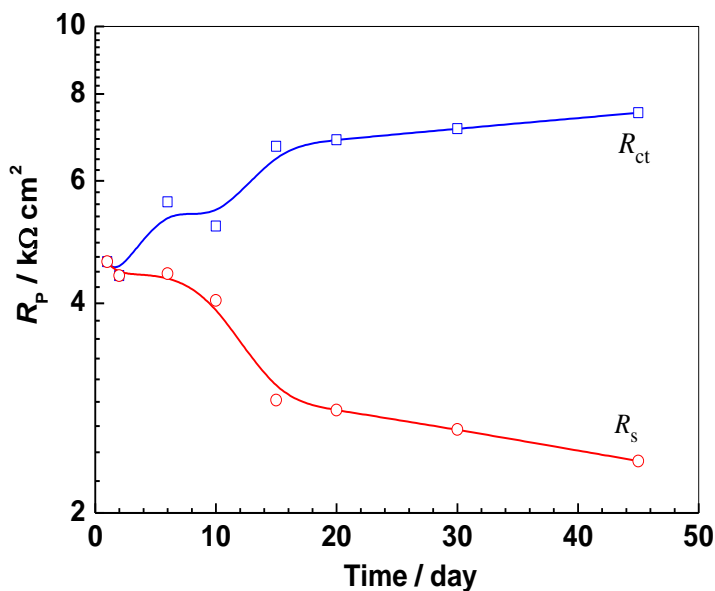


Figure 8. Evolution of the charge transfer resistance R_{ct} and the soil resistance R_s for X80 steel as a function of exposure period in the acidic soil. R_{ct} and R_s were obtained by fitting EIS plots using the equivalent electrical circuit shown in Fig. 7

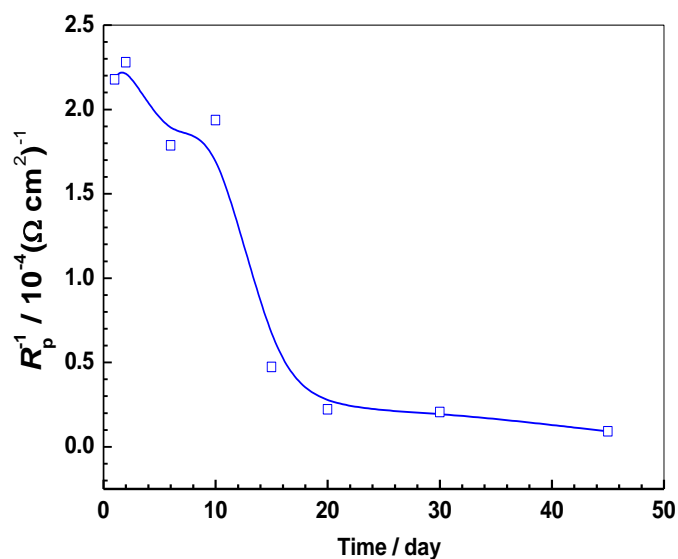


Figure 9. Evolution of the charge transfer resistance R_{ct} and the soil resistance R_s as a function of exposure time for the X80 steel in the acidic soil

The R_s has significantly high values in the range of 2.4–4.6 $\text{k}\Omega \text{ cm}^2$ over the test period and it decreases distinctly along with the exposure. This is attributed to physicochemical changes of the soil media around the electrode during the test. The conductivity of a soil varies greatly with the amount of dissolved ions in the soil, particularly for the highly resistive soil. The reduction or dissolution of the Fe oxide coating tends to cause the increase of the soil conductivity, as the results of the release of Fe^{2+} and negative-charge-bearing soil colloid particles [27]. Fe^{2+} and OH^- on the steel surface produced by corrosion process also results in increase of the soil conductivity.

3.5 Visual observation and surface analysis

The retrieved steel surface was covered by a black layer of corrosion product precipitate (Fe_3O_4) after 45 day exposure in the acidic soil, as optical observed in Fig. 10 a. After corrosion products were removed, typical morphology of corrosion attack of the steel surface was observed by SEM and the result is shown in Fig. 10 b. The steel surface undergoes severe *ulcerous* corrosion attack over the entire surface in the acidic soil.

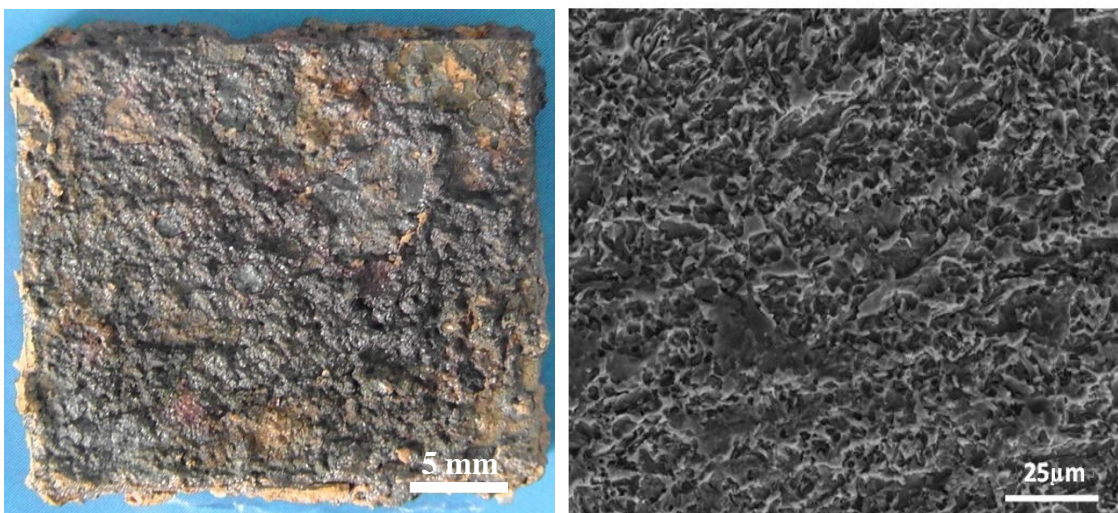


Figure 10. Optical appearance of corrosion products (a) and SEM morphology of corrosion attack of the steel surface (b) after 45 day exposure in the acidic soil

4. DISCUSSION

Metallic corrosion in soil is an electrochemical process in a thin moisture film adsorbed on the metal surface [28, 29]. The oxidant (or cathodic depolarizer) is necessary for corrosion process to proceed. It is generally granted that O_2 reduction acts as predominant cathodic process supporting soil corrosion [28, 30-33]. Aside from O_2 , a wide variety of alternative non-oxygen cathodic depolarizers has been recognized. Bicarbonate and CO_2 have been recognized as principal promoters of stress corrosion cracking (SCC) under disbonded coatings [34]. Nitrate and sulfate are cathodic depolarizers in the presence of bacteria, which have been commonly considered in soil corrosivity evaluation [35,

36]. However, O₂ diffusion through the acidic soil is extremely slow, owing to the heavy and sticky nature of the soil [37, 38]. It has also been evidenced that pH of the soil in the range of 5–8 is not a dominant factor influencing corrosivity [39, 40] and the pH itself cannot fully account for the high corrosivity of the acidic soil [8]. In summary, all the most common occurring oxidant mentioned above cannot account for the observed corrosivity of the acidic soil. Accordingly, it becomes essential to identify the existence of the possible oxidant and the corresponding cathodic process to better explain the electrochemical corrosion of pipeline steel in the acidic soil.

4.1 Specific of the acidic soil

Acidic soils, widely spread in subtropical/tropical area, are products of the intensive weathering and leaching process favored by abundant precipitation and good drainage in warm and humid climate condition [41]. The intensive weathering and leaching process decompose the primary minerals, accompanied by removal of most of weatherable minerals and soluble ions and by accumulation of secondary minerals that are stable and resistant to further weathering. The soil formation process endows the acidic soils with a series of specific properties, such as the kaolinite-dominated clay mineral, rich in Fe oxides, highly acidic, low soluble salt content and high resistivity, heavy and sticky texture, etc [9, 42].

Fe oxides are the most electrochemically active fraction of the acidic soil. Because of their high specific surface area, Fe oxides, even if present in only low concentrations, profoundly influence soil properties and play a significant role in various geochemical cycles of elements in natural environments. In this context, it is anticipated that the redox active Fe oxide should be a critical factor contributing to the high corrosivity of the acidic soils.

4.2 Electrode process of pipeline steel corrosion in acidic soils

The redox active Fe oxides participate in the cathodic reaction in corrosion process and are reduced to ferrous ion. The electrochemical process can be expressed as followings. For convenience, FeOOH is taken as an example of the soil Fe oxides.

Anode reaction:



Cathode reaction:



The effect of oxygen should also be taken into account in the long run of the corrosion process. During a period of low water content of the soil in the dry season, adventitious oxygen will diffuse into pores within the soil. In the O₂ rich environment, Fe²⁺ ions from reduction of soil Fe oxides or from corrosion product of the steel undergo re-oxidation and re-generation of Fe oxides occur through reactions with O₂ [43-45].



Accompanied with the re-oxidization of Fe^{2+} , the soil is re-acidified by the hydrolysis of ferric ions and subsequent precipitation of ferric hydroxide. The dynamic redox cycle of Fe oxides promotes and sustains corrosion process of the pipeline steel in acidic soils. The succession of wet and dry periods during alternation of seasons can sustain the “corrosion stimulating effect” of Fe oxides, which makes the soil more corrosion aggressive for the steel. The stimulating effect of a wet-dry cycle process on corrosion process in the acidic soil has been observed and is under investigation.

5. CONCLUSIONS

The corrosion dynamics and mechanism of pipeline steel in acidic soils are different from that in neutral/alkaline soils. The clay mineral of the acidic red soil collected from Yingtan, Southeast China is dominated by kaolinite with high content of Fe oxides and Al oxides. The presence of Fe oxides gives rise to new phenomena in soil corrosion that are worthy of consideration when assessing corrosivity of the soil. Fe oxides and their phase transformation should be concerned for better understanding corrosion in acidic soils. The steel surface undergoes severe corrosion attack over the entire surface in the acidic soil. Fe oxides and their phase transformation stimulate the electrochemical corrosion of the steel in the acidic soil. The reversible reduction and regeneration of soil Fe oxides form a dynamic redox cycle of Fe oxides, during which corrosion process of the steel is promoted. Further work are still required to exhibit more mechanistic details of the charge transfer process between Fe oxides and of the steel electrode.

ACKNOWLEDGEMENTS

The authors would like to thank Dr. Junhua Dong for suggestion on this study and Shuang Yang for help on electrochemical measurements. The authors are grateful to financially support from National Science Foundation of China (Grant No. 51131001), National R&D Infrastructure and Facility Development Program (Grant No. 2060503) and the Innovation Fund from IMR, CAS.

References

1. F.M. Song, *Corrosion*, 66 (2010) 035005-135005-12
2. M. Yan, J. Wang, E. Han, W. Ke, *Corros Sci*, 50 (2008) 1331-1339
3. M.C. Yan, J.Q. Wang, E.H. Han, W. Ke, *Corrosion Engineering Science and Technology*, 42 (2007) 42-49
4. A. Benmoussa, M. Hadjel, M. Traisnel, *Mater Corros*, 57 (2006) 771-777
5. R. Antunes de Sena, I.N. Bastos, G. Mendes Platt, *ISRN Chemical Engineering*, (2012) 103715 (103716 pp.)-103715 (103716 pp.)
6. Y.M. C, W.J. Q, H.E. H, S. C, K. W, *Acta Metallurgica Sinica*, 50 (2014) 1137-1145
7. I. Matsushima, Carbon Steel-Corrosion by Soils, in: R.W. Revie (Ed.) Uhlig's Corrosion Handbook, John Wiley & Sons, Inc., New York, 2000, pp. 555-560.
8. C.N. Cao, Material Corrosion in Natural Environment of China, Chemical Industry Press, Beijing, China, 2005.

9. Y.H. Wu, T.M. Liu, C. Sun, J. Xu, C.K. Yu, *Corrosion Engineering Science and Technology*, 45 (2010) 136-141
10. M. Yan, C. Sun, J. Xu, J. Dong, W. Ke, *Corros Sci*, 80 (2014) 309-317
11. M.C. Zhao, K. Yang, Y.Y. Shan, *Mater Lett*, 57 (2003) 1496-1500
12. J. Cui, J. Zhou, Y. Peng, Y.Q. He, H. Yang, L.J. Xu, A. Chan, *Environmental Science: Processes & Impacts*, 16 (2014) 1050-1058
13. S.S. Staff, *Keys to Soil Taxonomy 11th ed ed.*, United States Department of Agriculture, Natural Resources Conservation Service, Washington, DC, 2010.
14. I. Betova, M. Bojinov, P. Kinnunen, K. Mäkelä, T. Saario, *J Electroanal Chem*, 572 (2004) 211-223
15. D.E. J, J.M. Cowley, P.R. B, *Clay Clay Miner*, 48 (2000) 111-119
16. M. Barbalat, L. Lanarde, D. Caron, M. Meyer, J. Vittonato, F. Castillon, S. Fontaine, P. Refait, *Corros Sci*, 55 (2012) 246-253
17. S. Li, S. Jung, K.-w. Park, S.-M. Lee, Y.-G. Kim, *Materials Chemistry and Physics*, 103 (2007) 9-13
18. M. Urquidi-Macdonald, S. Real, D.D. Macdonald, *Electrochim Acta*, 35 (1990) 1559-1566
19. I. Nacic, D.D. Macdonald, *J Nucl Mater*, 379 (2008) 54-58
20. J. Ai, Y. Chen, M. Urquidi-Macdonald, D.D. Macdonald, *J Electrochem Soc*, 154 (2007) C43-C51
21. J. Xu, X. Wu, E.-H. Han, *Electrochim Acta*, 71 (2012) 219-226
22. S.N. Silva, L.F.P. Dick, *ECS Transactions*, 11 (2008) 35-40
23. R.N. Deo, N. Birbilis, J.P. Cull, *Corros Sci*, 80 (2014) 339-349
24. Y. Zhang, C. Yan, F. Wang, W. Li, *Corros Sci*, 47 (2005) 2816-2831
25. C. Thee, L. Hao, J. Dong, X. Mu, X. Wei, X. Li, W. Ke, *Corros Sci*, 78 (2014) 130-137
26. B. Rosborg, T. Kosec, A. Kranjc, J. Pan, A. Legat, *Electrochim Acta*, 56 (2011) 7862-7870
27. H. Dong, *Elemnets*, 8 (2012) 113-118
28. J. Jiang, J. Wang, W. Wang, W. Zhang, *Electrochim Acta*, 54 (2009) 3623-3629
29. I.S. Cole, D. Marney, *Corrosion Science*, 56 (2012) 5-16
30. C.P. Gardiner, R.E. Melchers, *Corros Sci*, 44 (2002) 2665-2673
31. C.P. Gardiner, R.E. Melchers, *Corros Sci*, 44 (2002) 2459-2478
32. J.N. Murray, P.J. Moran, *Corrosion*, 45 (1989) 34-43
33. S.K. Gupta, B.K. Gupta, *Corros Sci*, 19 (1979) 171-178
34. E.A. Charles, R.N. Parkins, *Corrosion*, 51 (1995) 518-527
35. D. Xu, Y. Li, F. Song, T. Gu, *Corros Sci*, 77 (2013) 385-390
36. S.Y. Li, Y.G. Kim, K.S. Jeon, Y.T. Kho, T. Kang, *Corrosion*, 57 (2001) 815-828
37. S.P. Bhattarai, D.J. Midmore, N. Su, *Biodiversity, Biofuels, Agroforestry and Conservation Agriculture*, in: E. Lichtfouse (Ed.) *Sustainable Agriculture Reviews*, Springer, Berlin, 2011, pp. 195-238.
38. P. Pernice, M. Arpaia, A. Costantini, *Mater Chem Phys*, 26 (1990) 323-330
39. A.I.M. Ismail, A.M. El-Shamy, *Appl Clay Sci*, 42 (2009) 356-362
40. A.M.A. Budiea, N. Yahaya, N.M. Nor, *International Journal of Civil & Environmental Engineering*, 12 (2012) 84-88
41. J.-Y. Li, R.-K. Xu, H. Zhang, *Journal of Soils and Sediments*, 12 (2012) 876-887
42. R. Xu, A. Zhao, Q. Li, X. Kong, G. Ji, *Geoderma*, 115 (2003) 75-84
43. T. Misawa, K. Hashimoto, S. Shimodaira, *Corros Sci*, 14 (1974) 131-149
44. L. Hao, S. Zhang, J. Dong, W. Ke, *Corros Sci*, 58 (2012) 175-180
45. H. Tamura, *Corros Sci*, 50 (2008) 1872-1883